Experimental demonstration of hybrid imaging for miniaturization of an optical zoom lens with a single moving element

Mads Demenikov,[1] Ewan Findlay,[2] and Andrew R. Harvey[1,*]

[1]*School of Engineering and Physical Sciences, Heriot Watt University, Edinburgh EH14 4AS, UK*

[2]*STMicroelectronics, 33 Pinkhill, Edinburgh EH12 7BF, UK*

**Corresponding author: a.r.harvey@hw.ac.uk*

Received September 20, 2010; revised January 13, 2011; accepted February 15, 2011; posted February 18, 2011 (Doc. ID 135455); published March 11, 2011

We experimentally demonstrate a miniaturized zoom lens with a single moving element based on the concepts and analysis described in Opt. Express **17**, 6118 (2009). We show that the implementation of either a cubic or a generalized cubic phase-modulation function makes miniaturization possible in addition to providing extended-depth-of-field imaging. We present recovered images for zoom lenses employing both phase-modulation functions and conclude that the generalized-cubic-phase function yields higher image quality without the artifacts present for the pure-cubic-phase function. © 2011 Optical Society of America

OCIS codes: 110.1758, 110.7348, 220.3620.

Mechanically compensated zoom lenses normally employ two moving elements: (a) a *variator*, which changes the lens focal length and hence "zooms" the lens, and (b) a *compensator*, which moves in an arc to compensate for the defocus introduced by the variator [1]. In traditional consumer mechanically compensated zoom lenses with large-format detectors and focal lengths in the region of a hundred millimeters, the defocus can be a few millimeters, and a cam can be used to control the movement of the compensator. With the recent trend toward smaller detectors, typical focal lengths have been reduced to a few millimeters; the length of the zoom lens is reduced to only a few centimeters; and the defocus is of the order of micrometers [1]. In such small zoom lenses, the cam needs to be replaced with a microstepper device whose actuation is determined by the variator position. The requirement for precise control of the compensator is a significant contribution to overall lens complexity and cost.

We have recently proposed that the defocus can be compensated by the implementation of an extended-depth-of-focus (EDOF) technique enabling the compensator to yield a zoom lens with only a single moving element (SME) and therefore reduced lens complexity and cost. As an example of EDOF, we proposed the introduction of a cubic-phase mask in the aperture stop combined with digital image restoration [1]; a technique commonly termed wavefront coding [2]. This technique has previously been used to mitigate aberrations other than defocus in a zoom lens with two moving elements [3]. For a SME zoom lens, however, the defocus increases with miniaturization, and for a length of 10 mm, it is of the order of micrometers or several waves of defocus [1] and may be mitigated using wavefront coding. In this Letter we demonstrate an example of a miniaturized SME zoom lens that employs wavefront coding to enable miniaturization to a length of ~11.5 mm. Based on the design layout in [1], we have optimized the design of the SME zoom lens shown in Fig. 1.

The SME zoom lens consists of a total of only five lens elements. Wavefront coding is introduced with a refractive phase-modulation function implemented on a 250-μm-thick phase plate in the aperture stop. The details of the optimized design are summarized in Table 1.

The optimized SME zoom lens introduces 5.5 λ of defocus for infinite-conjugate imaging at the midzoom position (the zoom position shown in Fig. 1), whereas it has zero defocus as the telezoom and wide-zoom positions. In general, the defocus can be efficiently mitigated by the use of a phase mask with a phase-modulation function of the form [4]

$$Z(X,Y) = \alpha(X^3 + Y^3) + \beta(X^2Y + Y^2X), \qquad (1)$$

where x and y are normalized coordinates of the aperture stop and α and β define the phase modulation. Two optimal combinations exist for α and β: a pure-cubic mask ($\beta = 0$) and a generalized-cubic phase mask with $\beta = -3\alpha$, which has threefold rotational symmetry [5]. These optimal solutions give the smallest rms error between the restored image and the object, for a given defocus, when the restoration kernel is identical to the defocused point-spread function (PSF) [5].

We have implemented both phase functions such that their EDOF imaging performance in the SME zoom lens can be compared. The implementation of wavefront coding involves trading off signal-to-noise ratio against insensitivity to defocus. A good tradeoff is obtained when the

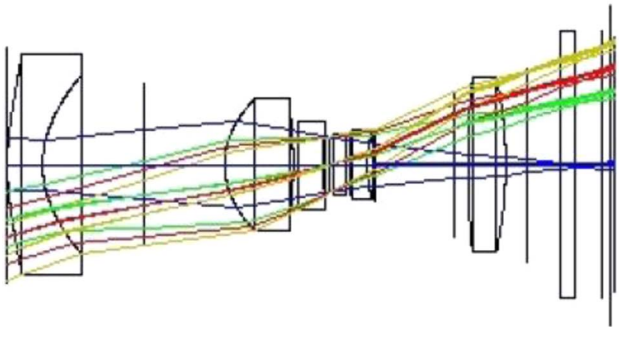

Fig. 1. (Color online) Optimized ray-traced zoom lens design.

 © 2011 Optical Society of America

Table 1. Zoom Lens Design Data

Zoom Lens Properties	
Total track	11.529 mm
Movement of lens group	2.9 mm
Zoom factor	2.3×
Aperture diameter	1.05 mm
Zoom Lens Configurations	
Tele-zoom position	$F/\# = 6.08$, EFL = 6.57 mm
Mid-zoom position	$F/\# = 4.31$, EFL = 4.24 mm
Wide-zoom position	$F/\# = 3.41$, EFL = 2.91 mm
Zoom Lens Elements	
Element 1	aspheric plastic lens
Element 2	aspheric plastic lens
Element 3	aspheric glass lens
Element 4	250 μm glass plate
Element 5	aspheric glass lens
Element 6	aspheric plastic lens
Sensor Dimensions	
Sensor format	2048 × 1536 square pixels
Pixel size	1.75 μm × 1.75 μm
Sensor size	3.584 mm × 2.688 mm

phase function is sufficiently strong to prevent excessive suppression of the modulation-transfer function (MTF) at all zoom positions for all spatial frequencies below the Nyquist sampling frequency of the detector, which for our system is 142 cycles per millimeter. We have determined that for the pure-cubic-phase function, $\alpha = 6.45\lambda$, corresponding to a peak-to-valley surface relief of 15.5 μm at 550 nm, is optimal. For the generalized-cubic optimum [5], we obtained $\alpha = 3.22\lambda$, which corresponds to a peak-to-valley surface relief of 10.87 μm.

The pure-cubic and generalized-cubic-phase masks were manufactured by laser polishing a fused silica glass plate with thickness of 250 μm, and they were located in the aperture stop of identical zoom lenses as shown in the ray trace in Fig. 1. A photograph of a manufactured zoom lens is shown in Fig. 2. The introduction of the phase function with a discrete phase mask is practical for appraisal purposes, but for optimal complexity reduction, the phase function should be implemented directly into the third element surface. Modeling indicates that the difference in performance between these two methods is insignificant.

Experimentally recorded PSFs at the three zoom positions—wide, mid, and narrow fields of view—were used as the basis for the image-recovery kernel. That is, variance of the PSF with zoom-related defocus is corrected in the image recovery. For each zoom position, a single kernel was used for all three-color planes and across the full field of view. PSFs were recorded with a color sensor for each zoom position by imaging a white-light, pinhole source at 1.2 m. The raw Bayer-format data were interpolated to three-color red–green–blue (RGB) format and then combined to yield a single gray-scale PSF for each zoom position tabulated in Table 1. Figure 3 shows the recorded PSFs for each zoom position: without phase modulation (that is, a simple flat mask at the aperture stop) in Figs. 3(a)–3(c), with pure-cubic phase modulation in Fig. 3(d)–3(f) and with generalized-cubic phase modulation in Figs. 3(g)–3(i).

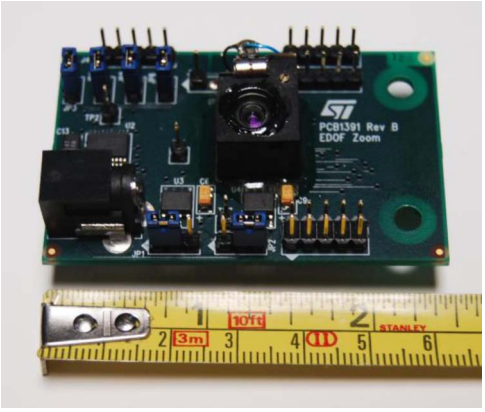

Fig. 2. (Color online) Manufactured zoom lens.

It can be seen from Fig. 3 that phase modulation has yielded the characteristic L-shaped and trefoil PSFs of the cubic- and generalized-cubic phase modulation, respectively, and that there is significant variation in the PSFs with the defocus accompanying zooming. The PSFs at wide-zoom (left column in Fig. 3) are slightly defocused because the variator was mechanically unable to move exactly to the end point nearest the detector. As reported in [1], whereas zeros in conventional defocused MTFs prevent restoration of high-quality images; for wavefront-coded systems there are no zeros, and hence restoration to a high-quality image is possible. A reduction in the variation in the PSF would be possible by increasing α; however a higher signal-to-noise ratio for the recovered image is possible by using a smaller value of α and accepting the corollary that the optimal image-recovery kernel is significantly different for each zoom position.

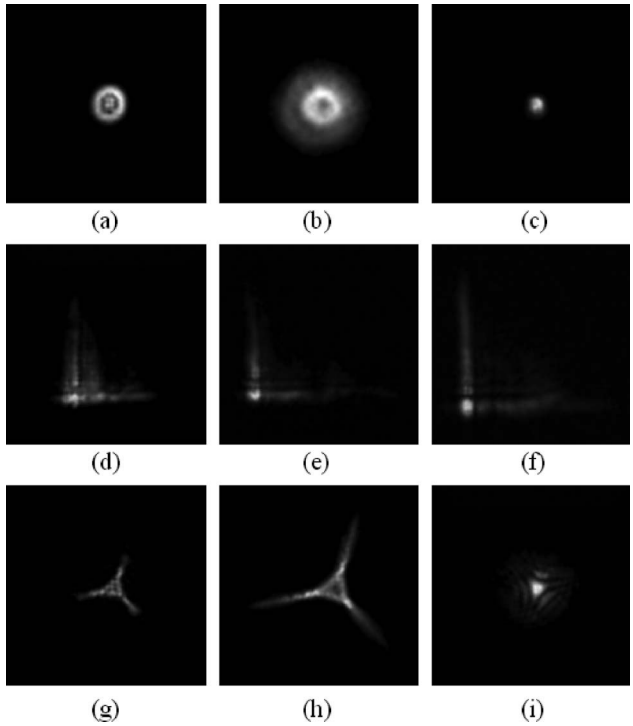

Fig. 3. (Color online) Recorded PSFs: Wide-zoom (left column), mid-zoom (middle column) and tele-zoom (right column) for a zoom lens with no phase modulation in the aperture stop (top row), pure-cubic modulation (middle row) and generalized-cubic modulation (bottom row).

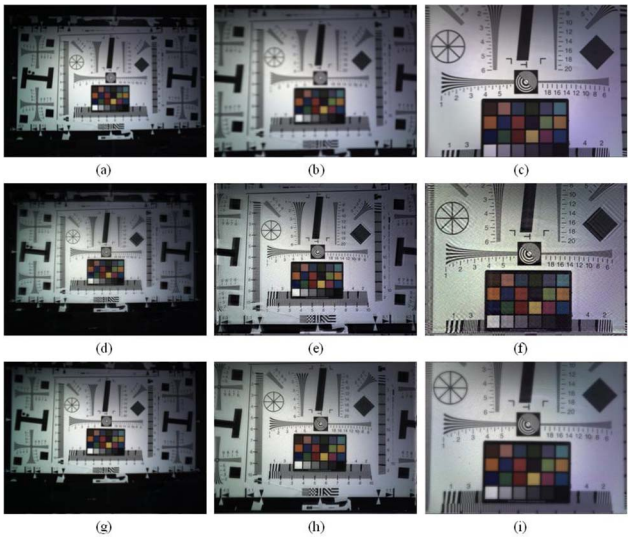

Fig. 4. (Color online) Images with SME lens (a)–(c) without phase mask, (d)–(f) with cubic phase mask and (g)–(i) with generalized-cubic phase mask.

The use of gray-scale kernels for restoration of color-images is common practice: each of the three RGB channels is restored here with the same gray-scale kernel and converted into a single color-image [6]. We present here a comparative assessment of the three zoom lenses for imaging a test chart at a displacement of 1.2 m. For the two wavefront-coded lenses, we apply image recovery using as the kernel the onaxis PSF corresponding to each zoom position, as shown in Fig. 3. For the conventional lens, without phase modulation, no image restoration is applied. The final images are shown in Fig. 4. For images recorded by the lens not employing wavefront coding, it can be seen that the images are of high quality at wide and narrow fields of view [Figs. 4(a) and 4(c)], but at mid field of view [Fig. 4(b)], the defocus associated with zooming ($W_{020} = 5\lambda$) leads to severe blurring; that is, because of severe suppression of the MTF at higher spatial frequencies [1].

By using the cubic or the generalized-cubic phase mask, we see that at the midzoom position, the images in Figs. 4(e) and 4(h) are much sharper than the one without a phase modulation [Fig. 4(b)]. The images obtained with the cubic-phase mask produce, however, replicationlike artifacts similar to those described in [7] across the sensor, whereas this is not the case for the generalized-cubic phase mask. These artifacts can be removed using an adaptive blind deconvolution algorithm [8], but because the generalized-cubic phase mask does not produce these artifacts, it is simpler to just use the generalized-cubic phase mask. Furthermore, we have found that, in common with earlier investigations into the application of wavefront coding to an IR singlet [9], the absence of nulls in the MTF for offaxis imaging yields higher overall image quality for the generalized-cubic mask than for the cubic mask. In conclusion, we have demonstrated that the miniaturized SME-zoom lens introduces defocus during the movement of the variator that is too large to be tolerated using traditional imaging, but that it can be optimally mitigated by use of a generalized-cubic phase mask and postdetection image recovery. We have thus demonstrated for the first time to our knowledge a practical implementation of a SME zoom lens. We presented as an example a zoom lens imaging at three fields-of-view: tele-, mid- and wide-zoom positions, where a matching restoration kernel was chosen for each zoom lens position. In principle, continuous zooming is possible with a finite number of image-recovery kernels that are approximately matched to the PSF at each zoom position and thus incurs the modest cost of a requirement for increased memory to store the multiple PSFs. For this particular lens, the $F/\#$, and hence the PSF, increases with zooming, and for a relative change of less than 5% in PSF size, which ensures small image quality degradation [7], continuous zooming requires 15 different kernels.

Overall, we have shown for the first time to our knowledge that reduction in lens length combined with relative simplicity of a SME zoom lens, by the use of a phase mask or other EDOF techniques, provides adequately high image quality and the potential for EDOF imaging.

We would like to thank Scottish Enterprise for funding.

References

1. M. Demenikov, E. Findlay, and A. R. Harvey, Opt. Express **17**, 6118 (2009).
2. E. Dowski and T. W. Cathey, Appl. Opt. **34**, 1859 (1995).
3. A. Prischepa and J. E. R. Dowski, Proc SPIE **4487**, 83 (2001).
4. S. Prasad, V. P. Pauca, R. J. Plemmons, T. C. Torgersen, and J. van der Gracht, Proc. SPIE **5559**, 335 (2004).
5. T. Vettenburg, N. Bustin, and A. R. Harvey, Opt. Express **18**, 9220 (2010)
6. Q. Shan, J. Jia, and A. Agarwala, in *SIGGRAPH '08: ACM SIGGRAPH 2008 Papers* (ACM, 2008), p. 1.
7. M. Demenikov and A. R. Harvey, Opt. Express **18**, 8207 (2010).
8. M. Demenikov and A. R. Harvey, Opt. Express **18**, 18035 (2010).
9. G. Muyo, A. Singh, M. Andersson, D. Huckridge, A. Wood, and A. R. Harvey, Opt. Express **17**, 21118 (2009).